ACS APPLIED MATERIALS & INTERFACES

Research Article

www.acsami.org

Structure and Properties of Polybenzimidazole/Silica Nanocomposite Electrolyte Membrane: Influence of Organic/Inorganic Interface

Shuvra Singha and Tushar Jana*

School of Chemistry University of Hyderabad Hyderabad 500046, India

Supporting Information

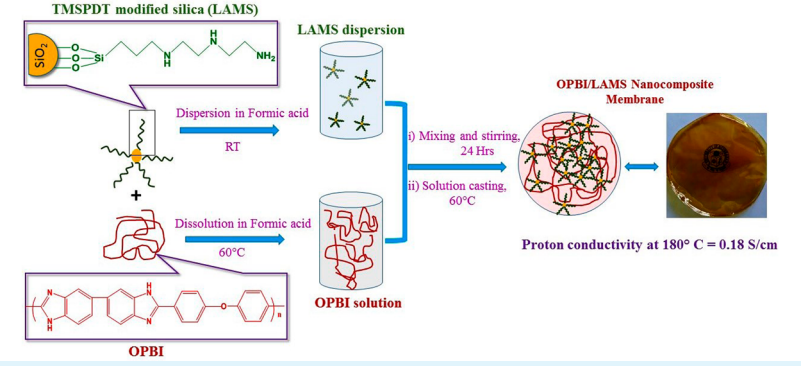

ABSTRACT: Although increased number of reports in recent years on proton exchange membrane (PEM) developed from nanocomposites of polybenzimidazole (PBI) with inorganic fillers brought hope to end the saga of contradiction between proton conductivity and variety of stabilities, such as mechanical, thermal,chemical, etc.; it still remains a prime challenge to develop a highly conducting PEM with superior aforementioned stabilities. In fact the very limited understanding of the interactions especially interfacial interaction between PBI and inorganic filler leads to confusion over the choice of inorganic filler type and their surface functionalities. Taking clue from our earlier study based on poly(4,4′-diphenylether-5,5′-bibenzimidazole) (OPBI)/silica nanocomposites, where silica nanoparticles modified with short chain amine showed interfacial interaction-dependent properties, in this work we explored the possibility of enhanced interfacial interaction and control over the interface by optimizing the chemistry of the silica surface. We functionalized the surface of silica nanoparticles with a longer aliphatic chain having multiple amine groups (named as long chain amine modified silica and abbreviated as LAMS). FTIR and ^{13}C solid-state NMR provided proof of hydrogen bonding interactions between the amine groups of modifier and those of OPBI. LAMS nanoparticles yielded a more distinguished self-assembly extending all over the OPBI matrix with increasing concentrations. The crystalline nature of these self-assembled clusters was probed by wide-angle X-ray diffraction (WAXD) studies and the morphological features were captured by transmission electron microscope (TEM). We demonstrated the changes in storage modulus and glass transition temperature (T_g) of the membranes, the fundamental parameters that are more sensitive to interfacial structure using temperature dependent dynamic mechanical analysis (DMA). All the nanocomposite membranes displayed enhanced mechanical, thermal and chemical stability than neat OPBI. The lower water uptake and swelling ratio and volume in both acid and water reflected the more hydrophobic characteristic of the nanocomposites. All the nanocomposite membranes showed phosphoric acid (PA) values to be higher than OPBI but the levels showed decreasing trend with increasing silica content; the reason attributed to the interparticle interaction. The self-assembled clusters of LAMS nanoparticles in the matrix created more sites for proton hopping as a result of which the proton conductivity of all the nanocomposites displayed an increasing trend.

KEYWORDS: *polymer nanocomposite, polybenzimidazole, interfacial interaction, proton exchange membrane, fuel cells*

INTRODUCTION

Incorporation of inorganic nanoparticles into proton exchange membranes (PEM) to substantially improve the properties and hence the capability of the membrane for high temperature fuel cell applications has been the subject of growing interest among many research groups.[1−5] Poly(4,4′-diophenylether-5,5′-bibenzimidazole) (OPBI) is an aryl ether linked polybenzimidazole, which, because of its unique materials properties like good solubility in low boiling solvents, high thermal stability, relatively low glass transition temperature, high modulus, toughness, etc., is widely studied for application in high temperature PEM fuel cells (HT-PEMFCs). Phosphoric acid (PA) doped OPBI exhibits high proton conductivity at temperatures above 100 °C. However, the chemical and

Received: September 12, 2014
Accepted: November 3, 2014
Published: November 3, 2014

Scheme 1. Preparation of OPBI/LAMS Nanocomposite Membrane

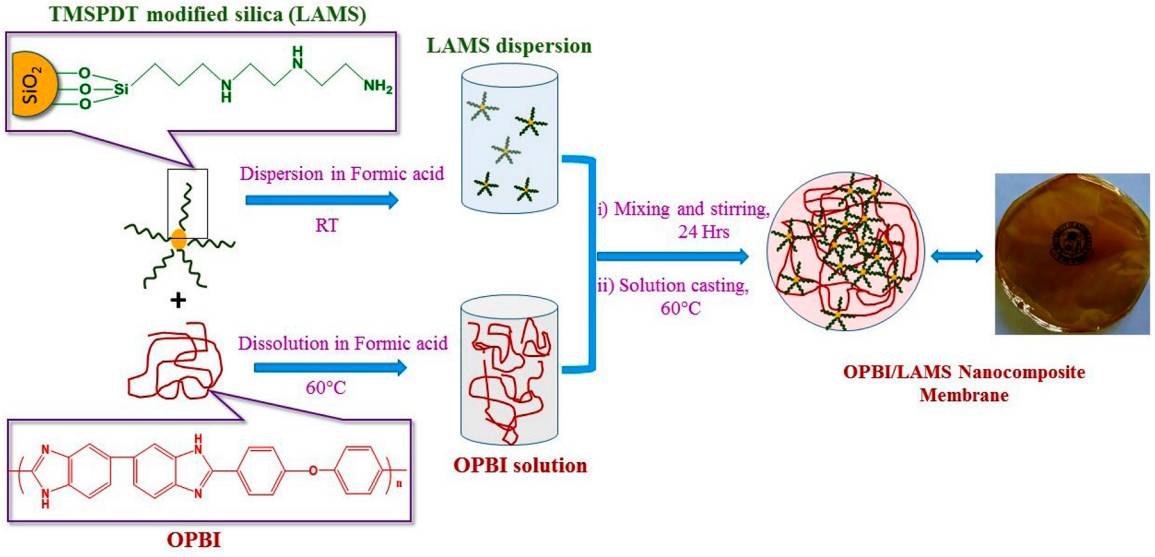

mechanical stabilities of PA doped OPBI tend to deteriorate significantly at higher temperatures. Hence, there occurs a trade-off between the acid doping level of the polymer membrane and its performance.[6,7] Recently we reported results describing the role of surface-modified silica and layered silicates in addressing the drawbacks of OPBI.[8,9] Nanocomposites of polybenzimidazole (PBI) with various nanofillers like TiO_2, graphene, carbon nanotubes, zeolites etc. have been reported by many groups.[10−14]

Among all the potential nanofillers, silica nanoparticles (NPs) are of particular interest because they offer easy surface modification. Surface chemical modification of nanoparticles is one aspect that plays a crucial role in determining the compatibility of the filler with the polymer, filler loading, dispersion quality, interfacial adhesion/interaction, extent of interphase, etc., factors that help in optimizing and designing polymer nanocomposites (PNCs) with desired properties.[15−18] There are many methods to tailor the surface of silica nanoparticles for them to mix well with the polymer matrix. Covalent attachment of short organic molecules like silane coupling agents is frequently used to functionalize the surface of silica. A new approach, that is gaining much popularity, is to covalently attach polymers to the surface via polymer grafting using controlled radical polymerization techniques like atom transfer radical polymerization (ATRP), reversible addition−fragmentation chain transfer (RAFT), click chemistry, etc.[19−21] The challenge, however, is to determine which interface structure suits best for obtaining PNCs with specific properties and for this, profound understanding of chemistry of filler surface is essential.

In our previous article, we prepared OPBI/silica nanocomposite demonstrating its feasibility for use as PEM in HT-PEMFCs.[9] We had modified the silica surface with 3-aminopropyltriethoxysilane (APTES), a short chain silane agent with a primary amine group. We noticed that the APTES modified silica NPs (or amine modified silica, abbreviated as AMS) formed a specific crystalline pattern (self-assembled super structures) in the polymer matrix but the same was not observed with the unmodified NPs, instead they were well dispersed. This long-range ordering of the surface modified silica NPs was attributed to the interactions between the functional groups on the filler surface and the functional groups of the polymer chains and also the interactions among the NPs themselves. This observation motivated us to study the interface chemistry of OPBI/silica nanocomposites further. Hence, in this article we modified the surface of silica NPs with *N*-(3-trimethoxysilylpropyl) diethylenetriamine (TMSPDT), a long chain silane agent with three amine functional groups (TMSPDT-modified silica nanoparticles will be called as long chain amine modified silica, abbreviated as LAMS henceforth), anticipating much better membrane properties that might arise because of the increased chain length and stronger multiple-point interaction between the three amine groups on the filler surface and the polymer matrix. Nanocomposite membranes having different weight percent of LAMS are fabricated and the effect of the structural interface on different properties related to fuel cell application is studied. We observed, from TEM images, a more robust self - assembly of the silica nanoparticles in the OPBI matrix and highly extended-structure morphology. This kind of patterning in the nanocomposites helped in increasing some of the properties further especially the proton conductivity while maintaining the structural integrity.

EXPERIMENTAL SECTION

The source of materials/reagents used in this study and polymer synthesis are included in the Supporting Information.

Silica Surface Functionalization. Silica nanoparticles were synthesized using Stöber's process described elsewhere,[22] and the average particle diameter was in the range of 50−60 nm. For surface functionalization, silica nanoparticles (0.5 g) were first dispersed in 60 mL of dry toluene. Then TMSPDT (12.0 mmol) was added dropwise to the dispersion and the mixture was refluxed for 24 h under dry nitrogen. The resulting long chain amine (TMSPDT) modified silica (LAMS) nanoparticles were then washed with methanol and acetone sequentially by using six centrifugation/redispersion cycles and then dried in vacuum oven at 60 °C for 12 h. The average particle size was in the range of 80−100 nm (as obtained from TEM images). Solid state ^{13}C NMR chemical shifts (respective carbon atoms are numbered and highlighted in bold italics font): δ 11.7 ppm (Si−***C(1)***H_2−CH_2−), 24.0 ppm (Si−CH_2−***C(2)***H_2−CH_2−), 42.9 ppm (Si−CH_2−CH_2−***C(3)***H_2−), 53.2 ppm (−NH−***C(4)***H_2−***C(5)***H_2−NH−***C(6)***H_2−***C(7)***H_2−NH_2).[23] The chemical shifts confirm the surface modification of silica with TMSPDT.

Fabrication of OPBI/LAMS Nanocomposite Membranes. Homogenous nanocomposite membranes were prepared by solution blending method by adding 4, 7, 10, and 15 wt % (with respect to polymer concentration) LAMS nanoparticles dispersion in formic acid to 2 wt % OPBI solution in formic acid. The final OPBI concentration in solution was 1 wt %. Then the solution was stirred vigorously at room temperature for 24 h to form a homogeneous mixture after which it was poured on to glass Petri dish and the solvent evaporated at 60 °C inside an oven slowly. The membranes that were formed were peeled off the petridish and were then dried in a vacuum oven at 100 °C to remove the trace solvent molecules. Nanocomposite membranes with unmodified silica (UMS), tht is, silica from Stöber's process, with exactly the same weight percent as LAMS were also prepared for comparison with OPBI/LAMS membranes. The preparation of OPBI/LAMS nanocomposite membranes is shown in Scheme 1.

Phosphoric Acid (PA) Doping of Nanocomposite Membranes. The thoroughly vacuum-dried OPBI and the nanocomposite membranes were immersed in phosphoric acid (85%) for 7 days to get free-standing PA doped films. After 7 days, the membranes were taken out from phosphoric acid (PA) bath, quickly wiped the surface-adsorbed PA, and then stored in zip-lock airtight packets for further analysis.

Characterization Methods. All the prepared nanocomposite membranes were characterized by several spectroscopic (FTIR, solid-state NMR), structural (wide-angle X-ray diffraction and transmission electron microscope), thermal (TG-DTA), and mechanical (dynamic mechanical analysis) techniques. The experimental details of which are given in Supporting Information. The detailed experimental procedure for PA loading, water uptake, swelling studies, and proton conductivity are also included in the Supporting Information.

RESULTS AND DISCUSSION

Spectroscopic Study. The incorporation of LAMS into OPBI matrix was analyzed by FT-IR and ^{13}C CPMAS solid state NMR (SS-NMR) spectra. Figure 1 shows the FT-IR spectra of OPBI, LAMS, and the nanocomposites.

As can be seen, the vibration at 1094 cm^{-1}, assigned to the Si−O−Si stretching frequency[24] of LAMS, appears in the spectra of all nanocomposite membranes and the absorption peak intensity increases with increase in the concentration of the filler in the matrix. This clearly suggests that the filler is coalesced with the polymer matrix. Also, OPBI shows three characteristic peaks at 3413, 3144, and 3066 cm^{-1} attributed to non-hydrogen bonded free N−H groups, self-associated hydrogen-bonded N−H groups and stretching modes of aromatic C−H groups, respectively.[25] On keen observation, we see that the intensity of peaks of N−H functionality decreases in the nanocomposite membranes, especially in the case of the membrane containing highest percentage of LAMS (15%), suggesting the formation of hydrogen bonds between amine groups of polymer and functional groups of LAMS.

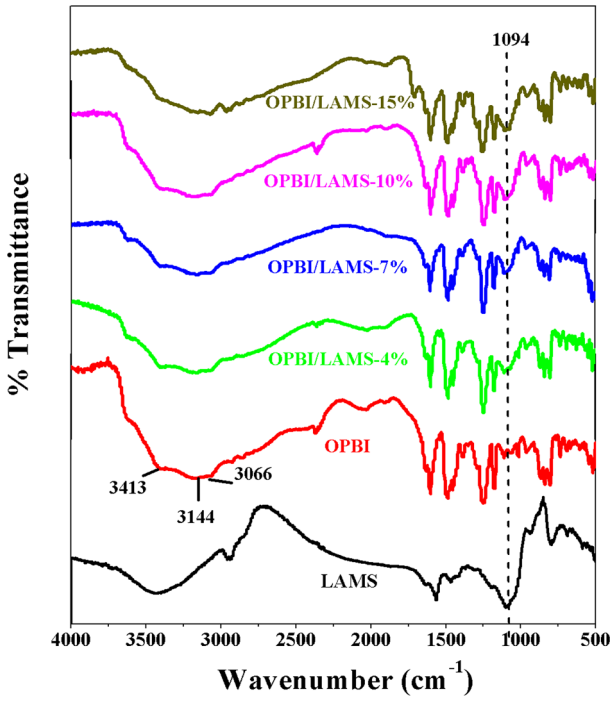

Figure 1. FTIR spectra of LAMS, OPBI, and OPBI/LAMS nanocomposite membranes at their indicated LAMS loadings.

The interactions between the filler and the polymer can be monitored by ^{13}C resonance shifts in the SS-NMR spectra of the nanocomposites. Figure 2 shows the ^{13}C CPMAS NMR spectra of OPBI, OPBI/LAMS-15%, and OPBI/UMS-15% nanocomposites. The peaks of OPBI are assigned with the corresponding numbers shown in the chemical structure. In OPBI spectrum, δ at 150 ppm (C1) corresponds to carbons of imidazole rings attached to phenylene ring, δ at 141 ppm (C2) is due to the carbons connecting the benzimidazole rings in the bibenzimidazole system and the one at 131 ppm (C3 and C4) comes from aromatic carbons bound to nitrogen atoms. The remaining shifts at 123 (C5−C8), 116 (C9 and C10), and 100 ppm (C 11) are due to the protonated carbons of the aromatic rings as assigned.[9,26] It has been shown in literature that TMSPDT molecules on silica surface show four ^{13}C resonance shifts (respective carbon atoms are highlighted in bold italics font) at 11.7, 24.0, 42.9 ppm corresponding to Si−***C***H_2−CH_2, CH_2−***C***H_2−CH_2, CH_2−***C***H_2−NH−, respectively, and at 53.2 ppm arising due to −NH−***C***H_2−***C***H_2−NH− and −NH−***C***H_2−***C***H_2−NH_2.[23] In the spectra of the nanocomposite films, we can see changes in the line shape and isotropic chemical shifts of OPBI, especially the peak due to carbon of imidazole (150 ppm) has shifted to 145 ppm in OPBI/LAMS-15% that clearly indicates intermolecular interactions between OPBI and functional groups of the filler. Further, the aforementioned peaks of TMSPDT have shifted to 14.2, 20.2, 30.5, and 39.2, respectively, confirming the presence of interaction between the silica surface and the OPBI matrix. It must be noted that in the case of unmodified silica (UMS) composite (OPBI/UMS-15%) there is no substantial change in the spectrum compared to OPBI and OPBI/LAMS membranes. This confirms the need for surface modification and also indicates the interaction between the polymer functional groups and silica surface functional groups.

Structure Evaluation. The structure of nanocomposites was further investigated by wide-angle X-ray diffraction (WAXD). Figure 3A and 3B show the WAXD patterns of pristine OPBI membrane, LAMS and UMS nanoparticles and the OPBI/LAMS, as well as OPBI/UMS nanocomposite membranes. OPBI shows a broad halo in the 2θ range 20° to 30° indicating its amorphous nature in accordance with literature.[8,9,25,26] The LAMS nanoparticles are also amorphous as seen from the broad featureless diffraction pattern in the figure. It is interesting to note that though both are amorphous in nature, the nanocomposite membranes, obtained by mixing the two, showed some sharp crystalline diffraction peaks, arising probably due to development of some kind of ordered arrangement in the polymer matrix. This crystallinity might be due to formation of certain discrete long-range ordering of LAMS nanoparticles in the matrix, brought about by the

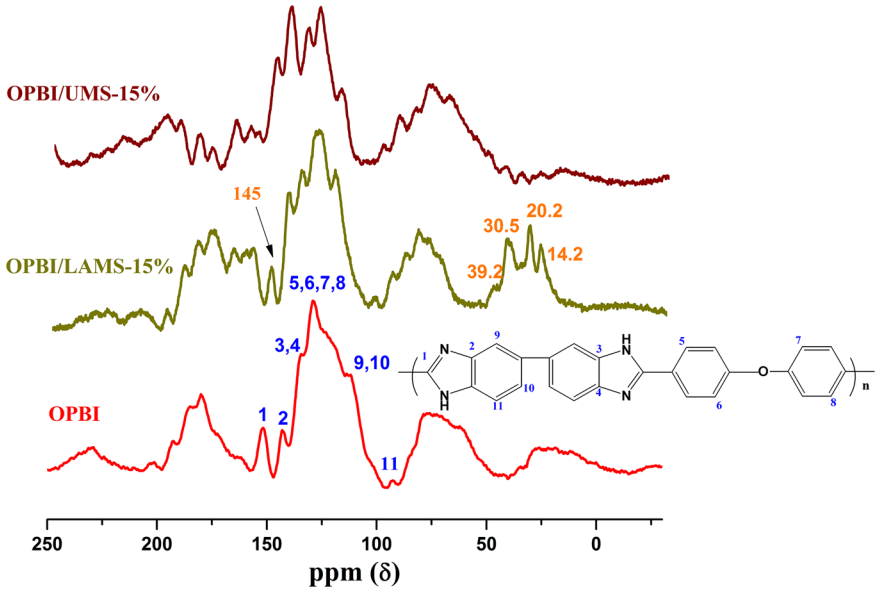

Figure 2. ^{13}C Solid-state NMR spectra of OPBI, OPBI/LAMS-15%, and OPBI/UMS-15% nanocomposite membranes.

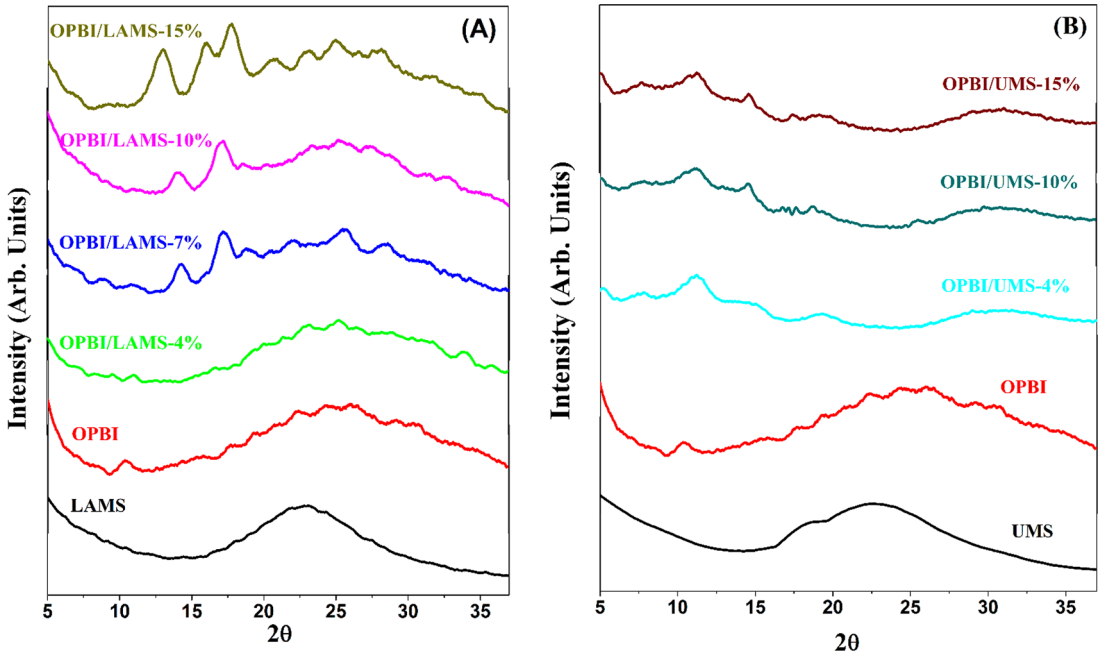

Figure 3. WAXD patterns of (A) OPBI/LAMS and (B) OPBI/UMS nanocomposites at their indicated loadings. OPBI, LAMS, and UMS patterns are included for comparison.

interplay of OPBI chains with the particles during membrane formation. In other words, the OPBI polymer chains, in an effort to interact with the functional groups of LAMS nanoparticles cause the latter to fall into an ordered arrangement in restricted pockets all over the matrix.[9,27] It is also worthwhile to note that, at lower filler loadings, there is no such crystalline ordering but as the filler concentration is increased gradually in the matrix the number of peaks increases and so do their sharpness. This suggests that the extent of the self-assembled super structures depends upon the percentage of filler loading. This phenomenon generates partial crystallinity in the polymer matrix in an otherwise amorphous polymer. The results are very similar to our previous work where the silica particles, decorated with amino propyl trimethoxysilane coupling agent, when mixed with OPBI gave rise to structural anisotropy. But we would like to emphasize that the formation of self-assembled clusters are more well-defined in this present work, as we will see from the TEM images in the next section. The presence of three amine functionality on the filler surface may be responsible for the stronger interaction with the OPBI matrix.

On the other hand, the OPBI/UMS (Figure 3B) nanocomposite membranes prepared in a similar fashion as the OPBI/LAMS membranes do not show any kind of sharp diffractions but only some broad amorphous peaks. This observation explains that the unmodified silica particles remain dispersed uniformly throughout the membrane and this fact coincides with the TEM images too. Though the surface

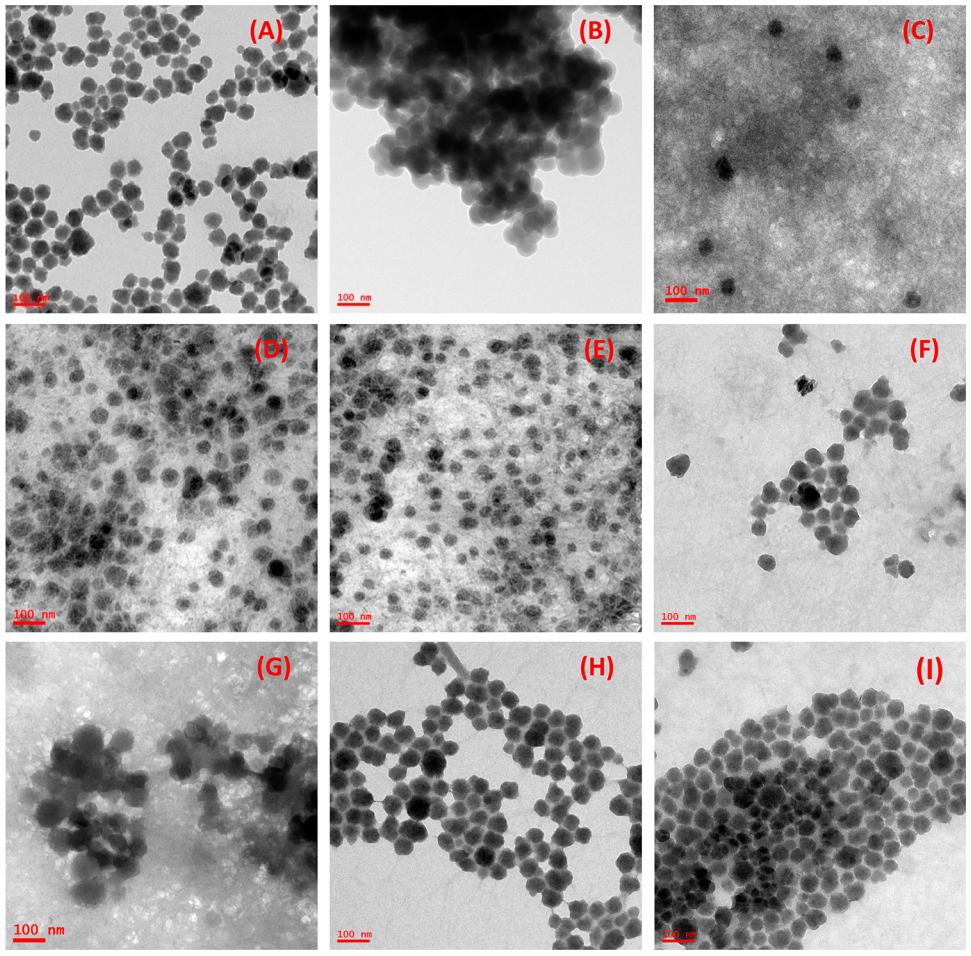

Figure 4. Transmission electron micrographs of (A) silica nanoparticles (UMS), (B) long chain amine modified silica nanoparticles (LAMS), the OPBI nanocomposites with (C) 4 wt %, (D) 10 wt %, (E) 15 wt % UMS loading, and (F) 4 wt %, (G) 7 wt % (H) 10 wt % (I) 15 wt % LAMS loading. The scale bar for all the images is 100 nm.

hydroxyl groups can interact with the polymer they are insufficient to interact so as to form crystalline structures and hence the membranes do not display distinct peaks. Hence the WAXD data leads us to understand that surface modification of silica nanoparticles plays a clear-cut role in shaping the structure and morphology of the nanocomposite membranes.

Transmission electron microscope (TEM) study reveals the surface morphology of the nanocomposite membranes. In Figure 4 TEM micrographs of UMS, LAMS nanoparticles and OPBI nanocomposites with UMS and LAMS at different percentage loadings are shown. We can see that the pristine silica particles appear spherical and are well dispersed and are in the size range of 50−60 nm. The surface modified silica particles, on the other hand, are agglomerated due to the extensive hydrogen bonding among the amine groups themselves, present in the TMSPDT chain. The average particle size measured from all over the grid was in the range of 80−100 nm. In the case of OPBI/UMS nanocomposites (Figure 4 C-E) we see that the silica particles are very well dispersed in the polymer matrix uniformly at lower as well as at higher concentration of the filler. But the OPBI/LAMS nanocomposites (Figure 4 F−I) show some kind of structural patterning of the silica particles in the matrix, very similar to our previous result where the particles were modified with a small chain amine moiety.[9] But in the present study the nanoparticles' self-assembling or the "coming-closer-to-each-other" process appears to be well maneuvered as seen from the images that show a definite arrangement of the filler particles at low as well as higher loadings, unlike in our previous result where the clustering appeared little messy, especially at higher concentrations. Also, at higher loadings of silica the patterning is such that it induces crystallinity in the matrix which is evident from the WAXD data that displays more number of sharp crystalline peaks for the 15% LAMS loaded OPBI membrane (Figure 4-I).

The reason for the formation of this robust self- assembled crystalline network is the presence of more number of functional groups (three amine groups in this study compared to only one in our previous study) on the surface of silica combined with long chain length of the modifier that helps in forming hydrogen bonds with the imidazole groups of OPBI more effectively at multiple points. As mentioned earlier, the LAMS nanoparticles, in the absence of polymer matrix, agglomerated together (Figure 4B) because of hydrogen bonding interactions among themselves but in the OPBI matrix they formed well-defined crystalline structure. This proves the higher affinity of the surfactant amine groups toward the imidazole groups of the polymer chains (adhesive interactions) than toward their own groups reiterating our claim that this is an important reason for the formation of strong self- assembled superstructures of the nanoparticles in the polymer matrix. Hence, we can say that we have tailored the

self-assembly of nanoparticles within the polymer matrix by tailoring the interface chemistry.

Thermal Stability. Figure 5 shows the thermograms of pristine OPBI along with the nanocomposite membranes and

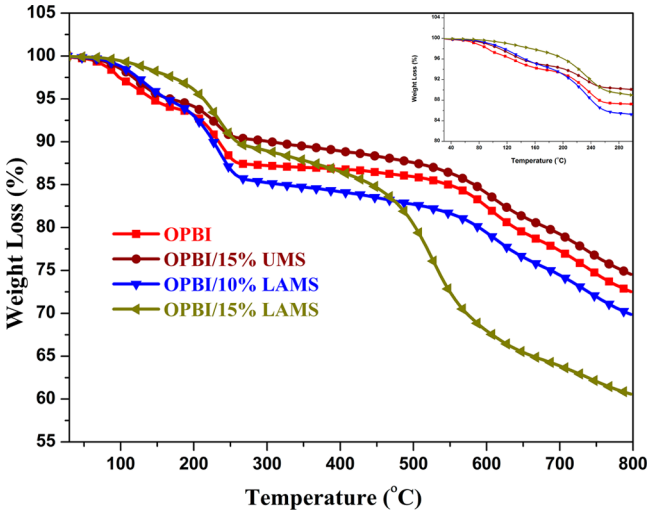

Figure 5. TGA plots of OPBI and its nanocomposite membranes with LAMS and UMS at their indicated loadings (inset shows TGA thermograms from RT to 300 °C).

inset figure shows the thermograms in the temperature window from RT to 300 °C to monitor the thermal changes in the membranes more carefully in that range (fuel cell operation temperature range). We performed the analysis under nitrogen atmosphere at a heating rate of 10 °C/min. The first weight loss, in the case of OPBI, of about 2−7% in the interval from room temperature to about 180 °C is reasonably due to loss of water molecules and the second weight loss starts from above 200 °C that is because of the degradation of the polymer chains. We can see from the figure that the thermal stability of OPBI/LAMS nanocomposite membranes, when compared to pristine OPBI, decreases after 200 °C. This is because of the decomposition of the long chain amine molecules present on the silica surface that adds to the degradation of the polymer chains and hence the 2−4% decrease in stability in the LAMS containing membranes; the degradation being more in OPBI/LAMS-15% membrane that contains the highest amount of LAMS. But the membrane containing UMS shows slightly increased thermal stability because a) it does not contain any organic modifier molecule (that can add to any decomposition) and b) silica particles themselves being highly thermally stable and well dispersed in the polymer matrix obviously tend to increase the stability of the membrane as a whole. Nevertheless, of particular interest, is the region from 100 to 200 °C which is the HT-PEMFC operating temperature region. All the nanocomposite membranes show an increased thermal stability than the neat OPBI, especially the OPBI/15% LAMS membrane that appears to be highly stable even up to 250 °C (inset of Figure 5). The weight loss percentage decreased from about 7% for the neat OPBI to just about 4% for the 15% LAMS containing membrane at 200 °C. This might be because of two reasons (a) the presence of silica particles helps in decreasing the moisture absorption tendency of the polymer membranes and (b) they act as thermal shields protecting the polymer chains from being subjected to heat. It is worthwhile to note that the 15%UMS containing OPBI membrane does not show any significant improvement (inset of Figure 5) in stability when compared to the effect that 15%LAMS imparts to OPBI. This suggests that the morphological patterning in the OPBI matrix by the LAMS particles might have a role to play in improving the thermal stability of the former. Hence the OPBI/LAMS nanocomposite membranes are very efficient for high temperature operating conditions.

Dynamic Mechanical Analysis. Shown in Figure 6A and 6B are the temperature dependent dynamic mechanical (storage modulus and tan δ) plots of the neat OPBI and its nanocomposites with LAMS. Plots of storage modulus as a function of temperature in Figure 6A show that OPBI nanocomposites containing 4% and 7% LAMS significantly enhance the dynamic storage moduli compared to the pristine OPBI which is attributed to the nano reinforcement provided by the nanofiller. But as we increase the concentration of the filler further the storage moduli tend to decrease. This might probably be because of the plasticizing nature of the modifier at higher loadings. In other words, beyond a certain concentration of the filler the reinforcing effect of the organic modifier on the silica surface is dominated by the plasticizing effect. The

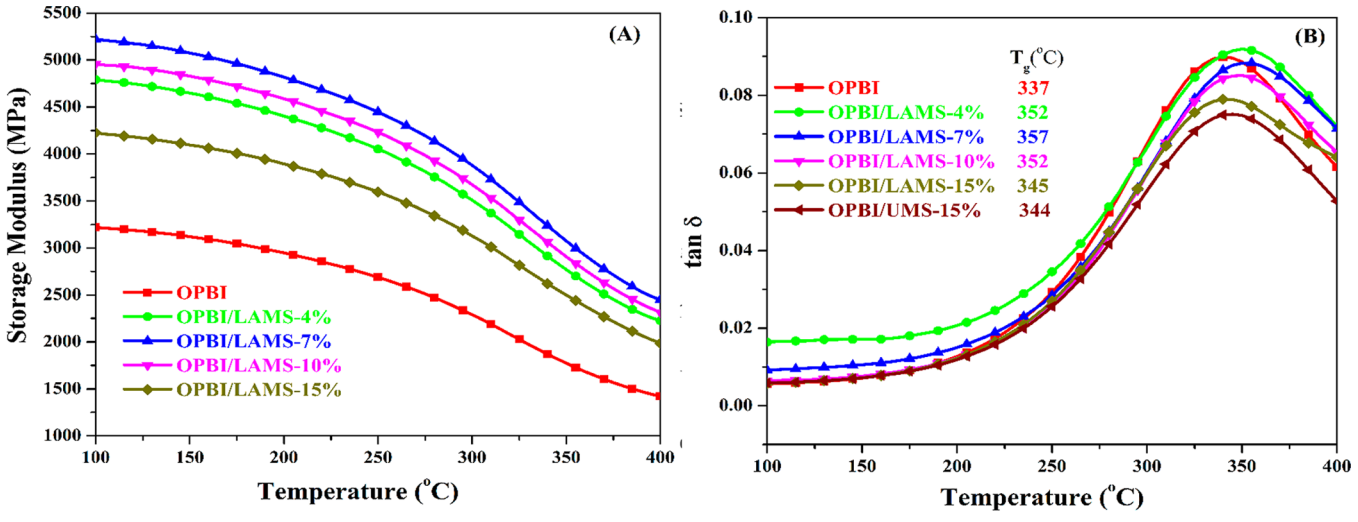

Figure 6. Temperature dependent (A) storage modulus and (B) tan δ plots of OPBI nanocomposites as obtained from DMA analysis.

effective immobilization of polymer chains occur only up to a certain threshold concentration of the modified silica beyond which, tht is, at 10% and 15% silica loading, the latter starts to induce softening of the polymer chains. Nevertheless, encouraging is the fact that the storage modulus (E') values are still higher (1.5 and 1.3 fold for 10% and 15% LAMS loading, respectively) than the neat OPBI indicating that the membranes are indeed suitable for high temperature PEM applications.

The tan δ plot in Figure 6B also follows the same pattern as the storage modulus. OPBI exhibits a well-defined relaxation peak at 337 °C that is assigned to the glass transition temperature (T_g) of the polymer chains. All the nanocomposites also show a single T_g. At lower filler formulations, i.e at 4% and 7%, the glass transition temperature show a shift in the peak maxima to higher temperature by 15 (to 352 °C) and 20 °C (357 °C), respectively, relative to neat OPBI. But when the percentage loading was raised to 10 and 15% the glass transition temperature started to decrease slowly as shown in Figure 6B. The reason for this anomaly, we believe, has to be associated with the morphology. That there is strong interaction between the long chain amine and the −N═ of PBI has been proved from spectroscopic data. This interaction introduces some kind of ordering of the nanoparticles in the polymer matrix as shown in our TEM images, as a result of which, at lower silica concentrations, the free volume of the polymer chains decreases significantly and so it takes a higher temperature to cause the free volume segmental mobility of the polymer chains, hence T_g increases. But at higher content of filler what happens is that the nanoparticles tend to come more closer to each other due to ionic interactions among themselves and form dense networks in the matrix, in such a way that the nanoparticles network is in contact with the polymer only from the periphery and not from within. Consequently the amount of interfacial area decreases; amount of bulk polymer is more compared to the amount of interfacial polymer (region where the polymer chains are stiffer). In other words polymer free volume increases. Hence a lower temperature would be sufficient to induce the segmental motion of the PBI chains. And so at higher concentrations (10% and 15%) of silica the T_g of OPBI decreases. Though we hypothesized that surface modification with LAMS nanoparticles might lead to higher T_g owing to the higher amount of interactions, contrarily we see decrease in the T_g at higher concentrations even after repeating the experiments several times. From these observations we would like to make a point that organic modification of nanofillers may not necessarily lead to property enhancement at all concentrations. Research in this area, type of organic modification of nanofillers and their effect on structure and property of the nanocomposite, is still in infancy and calls for serious attention to design materials with specifically required properties. But we must highlight that the T_g values for all the nanocomposites are higher than the pristine OPBI which shows that they are good enough to be used in HT-PEMFCs.

Oxidative Stability. To investigate the effect of peroxide radical attack on the chemical stability of the membranes they were immersed in Fenton's reagent (3% H_2O_2 containing 2 ppm $FeSO_4$) at 70 °C and the time when the membranes began to break into pieces was measured. Oxidative stability as a function of time has been plotted in Figure 7. All the nanocomposite membranes exhibit a higher chemical stability than the pure OPBI. Also, the stability increased with increase in concentration of silica in the matrix providing evidence that

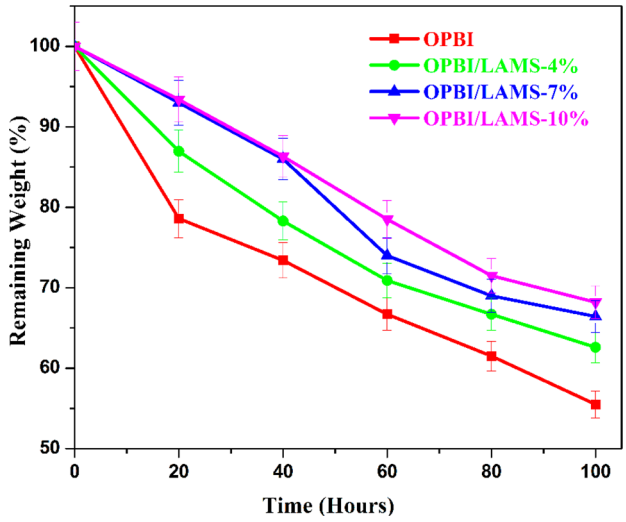

Figure 7. Oxidative stability of OPBI nanocomposite membranes with different percentage loadings of LAMS nanoparticles.

the LAMS particles protect the polar groups of OPBI from HO• and HOO• radicals' attack by forming networks all over the matrix. The enhanced oxidative resistance may be attributed to the hydrogen bonding interactions between the TMSPDT on silica surface and the OPBI chains. At higher silica content, there are more ionic interactions and hence better shielding of polymer chains, thus improving their durability in an oxidative atmosphere and making these nanocomposite membranes suitable for PEM applications.

Water Uptake, Swelling Ratio, Swelling Volume in Water and PA, and PA Doping Level. It is widely known that OPBI is hydrophilic and has high affinity for moisture due to the tendency of −N═ atom to form hydrogen bonds with water molecules.[28,29] After immersion of the membrane in distilled water for 3 days, we found that OPBI can absorb about 25 wt % of water with respect to dry membrane. From Table 1,

Table 1. Water Uptake, Swelling Ratio, and Volume in Water of OPBI and Nanocomposite Membranes at Indicated Loadings[a]

sample	water uptake (%)	swelling ratio (%)	swelling volume (%)
OPBI	25.00 (6.75)	5.57 (0.05)	12.13 (5.11)
OPBI/LAMS-4%	20.04 (1.94)	5.34 (0.28)	10.9 (3.28)
OPBI/LAMS-7%	17.55 (0.75)	4.93 (0.10)	9.92 (0.16)
OPBI/LAMS-10%	14.99 (1.68)	4.75 (1.88)	8.58 (1.53)
OPBI/LAMS-15%	14.51 (0.19)	4.46 (0.15)	8.12 (0.11)

[a]The standard deviation of measurements is shown in parentheses.

we can see reduction in the water uptake capacity of all the nanocomposite membranes and it decreases with increasing silica content. This is evident even from the TGA plots (inset of Figure 5) which show a decrease in initial weight loss percentage with increasing LAMS content in the matrix. Also, since the −N═ atom of OPBI might be involved in hydrogen bonding with the TMSPDT chains on silica surface the chances of water molecules getting bonded to the −N═ decreases—more filler content results in more OPBI chains associated with TMSPDT chains—hence the lower water uptake.

As expected, the swelling ratio and volume percentage of the nanocomposite membranes in PA follow a pattern similar to

that in water. The values are tabulated in Table 2. The presence of silica nanoparticles in polymer matrix would prevent the

Table 2. Swelling Ratio and Swelling Volume of OPBI and Nanocomposite Membranes in Phosphoric Acid[a]

sample	swelling ratio (%)	swelling volume (%)
OPBI	5.42 (1.26)	475 (6.55)
OPBI/LAMS-4%	3.32 (0.12)	480 (2.66)
OPBI/LAMS-7%	3.99 (0.15)	425 (3.48)
OPBI/LAMS-10%	1.90 (0)	379 (1.12)

[a]The standard deviation of measurements is shown in parentheses.

motion of OPBI chains and makes them rigid, thus preventing the separation between the stacked polymer backbones caused by the doping acid. Hence an increment in silica loading helps in controlling the swelling of the nanocomposite membranes.

Table 3 compares the acid doping level of OPBI with OPBI/LAMS nanocomposite membranes. The data show that the PA

Table 3. PA Doping Levels of OPBI and Nanocomposite Membranes at Their Indicated Loadings[a]

sample	no. of mol/OPBI repeat unit
OPBI	21.8 (1.05)
OPBI/LAMS-4%	26.7 (1.40)
OPBI/LAMS-7%	25.3 (0.28)
OPBI/LAMS-10%	24.3 (0.23)
OPBI/LAMS-15%	23.4 (0.28)
OPBI/UMS-15%	26.6 (1.96)

[a]The standard deviation of measurements is shown in parentheses.

doping level of the nanocomposite membranes is higher than the parent polymer but decreases slightly for higher LAMS concentration in the matrix. The number of moles of PA per repeat unit (RU) for pure OPBI is 21.8. The level increases to 26.7 mol/RU with 4% silica loading from where it decreases to 23.4 mol/R.U with 15% of the filler. At low silica content though the TMSPDT molecules are involved in hydrogen bonding with OPBI chains some of the −NH− moieties are available in excess which would contribute to higher acid uptake by the nanocomposite membranes. But as the silica nanoparticles' loading is increased they start forming dense networks all over the matrix and hence more number of OPBI chains would be involved in bonding with the modifier chains because of which bonding with PA molecules would be comparatively lesser. And thus the PA uptake of the nanocomposite membranes decreases slightly with increasing filler loading. This is not a concern for the use of these nanocomposite membranes as PEM in high temperature applications as the values are still higher than neat OPBI. From these observations we can remark that these OPBI/LAMS nanocomposite membranes do have a lot of potential to be used in HT-PEMFCs. But the OPBI/UMS-15% membrane shows high PA doping level because of the polar −OH groups on silica that are able to hold more acid molecules. Nevertheless, this fact does not hold much significance since the membrane shows lower proton conductivity as we will see in the next section.

Proton Conductivity. As described in the experimental section (Supporting Information) all the membranes were dried by heating at 100 °C prior to the start of the measurement to avoid the effect of moisture. Therefore, all the data presented in this section are the results obtained from second heating cycle. The proton conductivity, as a function of temperature, of OPBI and all the nanocomposite membranes was measured in a closed chamber without any external humidification. Figure 8 shows the conductivity plots of the

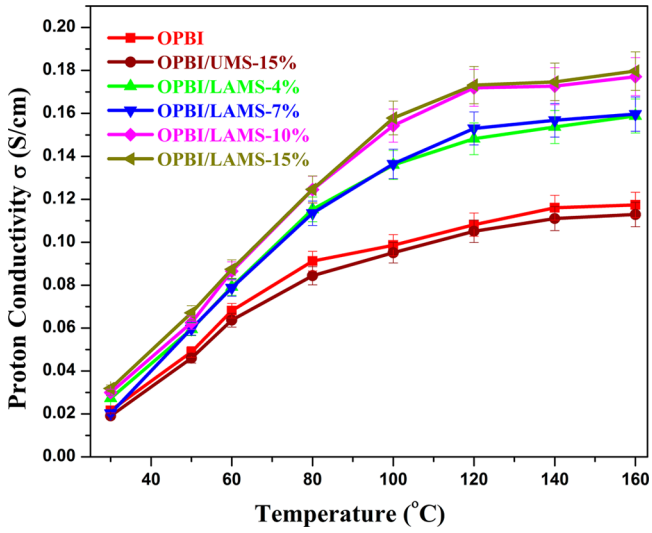

Figure 8. Proton conductivity against temperature of OPBI and OPBI/LAMS nanocomposite membranes at their indicated filler loading.

membranes. The LAMS containing nanocomposite membranes show significant increase in proton conductivity compared to neat OPBI membranes and it enhances with increasing LAMS loading. At 160 °C, the conductivity of OPBI/LAMS-15% is 0.181 S/cm, an increase by more than 1.5-fold, compared to that of OPBI for which the value is 0.118 S/cm. In our previous paper, we reported that the APTES modified silica nanocomposite membranes showed increase in conductivity with increasing filler loading because of the enhanced PA doping level of the nanocomposite membranes.[9] But in this study it is interesting to note that the proton conductivity data of OPBI/LAMS nanocomposite membranes is quite in contrast to their PA doping levels; as the LAMS content is increased from 4% to 15% the PA doping levels decreases (though gradually) but the conductivity shows an increasing trend. It is a known fact that PBI membranes with high acid doping levels tend to deteriorate at higher temperatures because of plasticizing nature of the doped acid.[30,31] Hence, in this regard, the high conductivity values obtained with lower (or decreased) doping levels in the membranes with high filler content provides additional benefits. The reason for this behavior, again, is attributed to the role of the surface modifier molecules in forming structural networks. As already explained the TMSPDT chains, with three amine groups, on silica surface are hydrogen bonded to the OPBI chains and form crystallites all over the matrix. This crystal formation in turn provide proton conducting channels in the matrix that helps in easier and efficient proton hopping across the membrane. On the other hand, the OPBI/UMS-15% nanocomposite membrane, despite having the highest PA doping level, shows the least conductivity among all the membranes (even lower than pristine OPBI) with a value at 0.111 S/cm. As mentioned earlier, the UMS particles are well dispersed all over the matrix and can hold more acid due to the −OH groups. But the conduction of protons is relatively much lower. This is because the bare silica particles do not create any

proton conducting pathways. Instead, they act as barriers that cause tortuosity of the diffusive path for the penetrating protons. And so the protons are forced to wiggle around the particles traveling through a tortuous path thereby decreasing the proton transfer efficiency.[14,32,33] This phenomenon reinforces the importance of the interface chemistry that plays a crucial role in facilitating easy and efficient ion transport in the case of LAMS modified silica nanocomposite membranes—hydrogen bonding interactions between OPBI and the surface modifier molecules offers more hopping sites for conduction of the ionized protons.

For hopping-like conduction mechanism dependent on temperature, conductivity follow Arrhenius equation[34,35]

$$\ln(\sigma T) = \ln \sigma_o - \frac{E_a}{RT} \quad (1)$$

Where σ is the proton conductivity of the membrane (S cm^{-1}), σ_o is the pre-exponential factor (SK^{-1} cm^{-1}), E_a is the proton conducting activation energy (kJ mol^{-1}), R is the ideal gas constant (J mol^{-1}K^{-1}) and T is the temperature (K). E_a, which is the minimum energy required for proton conduction, is obtained from the slope of linear fit of eq 1. The Arrhenius plots of acid doped OPBI and all the OPBI/LAMS nanocomposite membranes are illustrated in Figure 9. The data fit

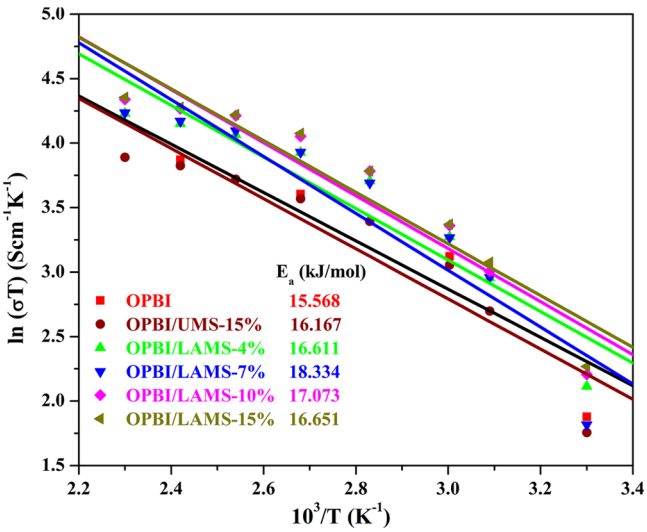

Figure 9. Arrhenius plots for the proton conduction of OPBI and nanocomposite membranes at indicated loadings.

fairly well the Arrhenius equation which implies that the proton transport is mainly regulated by Grotthus mechanism occurring as a result of proton hopping between protonated site of polymer chains and nonprotonated sites of the modifier chains or vice versa. But in the case of nanocomposites there are some irregularities from linear shape of the plots and this might suggest that proton conduction is partly contributed by Vehicular mechanism as well - the self- assembly of the LAMS nanoparticles via hydrogen bonding helps in self-diffusion of the protons through the conducting channels created by the former. The E_a values of the nanocomposite membranes are slightly higher than the pure OPBI and this is obvious because the nanofiller acts as carrier-bridge for protons and this process demands more energy.

Comparative Study of OPBI Nanocomposite Membranes Made from Long-Chain Amine Modified Silica (LAMS) to Short-Chain Amine Modified Silica (AMS). Since proton conductivity and acid doping level are the two important parameters that determine the fate of PEM in a fuel cell, we would like to make a comparison to show how the surface modification of silica nanoparticles can influence these two properties. The proton conductivity value at 160 °C and the PA doping level of each of 4, 7, and 10 wt % nanofiller loading of OPBI/AMS and OPBI/LAMS nanocomposite membranes are tabulated in Table 4.

We can observe, from Table 4, that there is a clear increment in the PA doping level and proton conductivity value at 160 °C for the OPBI/LAMS nanocomposite membranes compared to those of OPBI/AMS membranes. As discussed earlier, though both AMS and LAMS modified silica nanoparticles self-assemble in the OPBI matrix, the self-assembly is more ordered and robust in the case of OPBI/LAMS membranes owing to the long chain and multiple interaction points of LAMS molecules. And this comparative chart once again confirms this assertion of ours. This table also provides proof of our claim that silica modification with LAMS moiety provide more proton hopping sites than with AMS molecules, thereby increasing the proton conductivity of the membranes. Thus, surface modification of silica nanoparticles indeed plays a very important role in enhancing the properties of OPBI.

CONCLUSION

A series of nanocomposite membranes of OPBI with long chain amine modified silica (LAMS) nanoparticles are prepared with an objective to study the effect of particle surface modification, loading and filler/matrix interactions on the bulk properties of nanocomposite membrane. Spectroscopic studies clearly prove the interaction between the functionalities of OPBI and LAMS. The varying degree of dispersion with increase in weight percent of the nanoparticles is examined using X-ray diffraction and morphology using TEM images which show structural ordering of nanoparticles. The DMA results indicate that dispersion pattern affects the T_g and the mechanical reinforcement is dependent on the interaction of the nanoparticles not only with the matrix but also among themselves at higher concentrations, where, the particle—particle interaction is more than the particle—matrix interaction. The inclusion of LAMS in

Table 4. Comparison of Proton Conductivity (at 160°C) and PA Doping Level of OPBI/LAMS and OPBI/AMS Nanocomposite Membranes

	proton conductivity at 160 °C (S/cm)		PA doping level (mol/RU)	
nanofiller loading (wt %)	OPBI/AMS nanocomposite[a]	OPBI/LAMS nanocomposite	OPBI/AMS nanocomposite[a]	OPBI/LAMS nanocomposite
4	0.062	0.157	21.75	26.7
7	0.073	0.159	22.75	25.3
10	0.093	0.176	24.43	24.3

[a]These data are obtained from our previous study.[9]

the matrix leads to elevation of the thermal and oxidative stability of the nanocomposite membranes. Water uptake, swelling ratio and swelling volume in both PA and water shows promising results. The hydrogen bonding interaction between PBI and LAMS create proton conducting channels that is responsible for the higher conductivity of the nanocomposite membranes which is not observed in the case of unmodified silica (UMS) loaded membranes. While the findings in this study demonstrates the potential of OPBI/LAMS nanocomposite membranes for use as PEM in fuel cells, it also emphasizes the need for further study using different aliphatic chain length silane coupling agents as modifiers in order to understand better the underlying chemistry governing interfaces so as to design materials with desired behavior.

■ ASSOCIATED CONTENT

Supporting Information

Experimental section and characterization methods, FTIR, ^{13}C solid-state NMR, WAXD, TEM, TGA, DMA, oxidative stability, PA doping level, water uptake, swelling ratio, swelling volume, and proton conductivity measurement. This material is available free of charge via the Internet at http://pubs.acs.org.

■ AUTHOR INFORMATION

Corresponding Author

*(Tel: (+91) 40 23134808. Fax: (+91) 40 23012460. E-mail: tusharjana@uohyd.ac.in tjscuoh@gmail.com.

Notes

The authors declare no competing financial interest.

■ ACKNOWLEDGMENTS

We gratefully acknowledge financial support by SERB, Govt. of India (Project No. SB/S1/PC-054/2013). We sincerely thank Mr. Durgaprasad, Centre for Nanotechnology, University of Hyderabad for helping us with the TEM studies. S.S. thanks CSIR for the senior research fellowship.

■ REFERENCES

(1) Hickner, M. A. Proton Exchange Membrane Nanocomposites. *Functional Polymer Nanocomposites for Energy Storage and Conversion*; American Chemical Society: Washington, DC, 2010; Chapter 11, pp 155−170.

(2) Nagarale, R. K.; Shin, W.; Singh, P. K. Progress in Ionic Organic−Inorganic Composite Membranes for Fuel Cell Applications. *Polym. Chem.* **2010**, *1*, 388−408.

(3) Sanchez, C.; Belleville, P.; Popall, M.; Nicole, L. Applications of Advanced Hybrid Organic Inorganic Nanomaterials: From Laboratory to Market. *Chem. Soc. Rev.* **2011**, *40*, 696−753.

(4) Tripathi, B. P.; Shahi, V. K. Organic−Inorganic Nanocomposite Polymer Electrolyte Membranes for Fuel Cell Applications. *Prog. Polym. Sci.* **2011**, *36*, 945−979.

(5) Laberty-Robert, C.; Vallé, K.; Pereira, F.; Sanchez, C. Design and Properties of Functional Hybrid Organic−Inorganic Membranes for Fuel Cells. *Chem. Soc. Rev.* **2011**, *40*, 961−1005.

(6) Zhang, H.; Shen, P. K. Recent Development of Polymer Electrolyte Membranes for Fuel Cells. *Chem. Rev.* **2012**, *112*, 2780−2832.

(7) Asensio, J. A.; Sánchez, E. M.; Gómez-Romero, P. Proton-conducting Membranes based on Benzimidazole Polymers for High-Temperature PEM Fuel Cells. A Chemical Quest. *Chem. Soc. Rev.* **2010**, *39*, 3210−3239.

(8) Ghosh, S.; Sannigrahi, A.; Maity, S.; Jana, T. Role of Clays Structures on the Polybenzimidazole Nanocomposites: Potential Membranes for the Use in Polymer Electrolyte Membrane Fuel Cell. *J. Phys. Chem. C* **2011**, *115*, 11474−11483.

(9) Ghosh, S.; Maity, S.; Jana, T. Polybenzimidazole/Silica Nanocomposites: Organic−Inorganic Hybrid Membranes for PEM Fuel Cell. *J. Mater. Chem.* **2011**, *21*, 14897−14906.

(10) Pu, H.; Liu, L.; Chang, Z.; Yuan, J. Organic/Inorganic Composite Membranes based on Polybenzimidazole and Nano-SiO_2. *Electrochim. Acta* **2009**, *54*, 7536−7541.

(11) Liu, Y.; Shi, Z.; Xu, H.; Fang, J.; Ma, X.; Yin, J. Preparation, Characterization, and Properties of Novel Polyhedral Oligomeric Silsesquioxane-Polybenzimidazole Nanocomposites by Friedel-Crafts Reaction. *Macromolecules* **2010**, *43*, 6731−6738.

(12) Suryani; Chang, C.; Liu, Y.; Lee, Y. M. Polybenzimidazole Membranes Modified with Polyelectrolyte-functionalized Multiwalled Carbon Nanotubes for Proton Exchange Membrane Fuel Cells. *J. Mater. Chem.* **2011**, *21*, 7480−7486.

(13) Wang, Y.; Shi, Z.; Fang, J.; Xu, H.; Ma, X.; Yin, J. Direct Exfoliation of Graphene in Methanesulfonic Acid and Facile Synthesis of Graphene/ Polybenzimidazole Nanocomposites. *J. Mater. Chem.* **2011**, *21*, 505−512.

(14) Namazi, H.; Ahmadi, H. Improving the Proton Conductivity and Water Uptake of Polybenzimidazole-based Proton Exchange Nanocomposite Membranes with TiO_2 and SiO_2 Nanoparticles Chemically Modified Surfaces. *J. Power Sources* **2011**, *196*, 2573−2583.

(15) Zou, H.; Wu, S.; Shen, J. Polymer/Silica Nanocomposites: Preparation, Characterization, Properties, and Applications. *Chem. Rev.* **2008**, *108*, 3893−3957.

(16) Yang, J.; Deng, L.; Han, C.; Duan, J.; Ma, M.; Zhang, X.; Xu, F.; Sun, R. Synthetic and Viscoelastic Behaviors of Silica Nanoparticle Reinforced Poly (acrylamide) Core−Shell Nanocomposite Hydrogels. *Soft Matter* **2013**, *9*, 1220−1230.

(17) Kumar, S. K.; Jouault, N.; Benicewicz, B.; Neely, T. Nanocomposites with Polymer Grafted Nanoparticles. *Macromolecules* **2013**, *46*, 3199−3214.

(18) Li, Y.; Krentz, T. M.; Wang, L.; Benicewicz, B. C.; Schadler, L. S. Ligand Engineering of Polymer Nanocomposites: From the Simple to the Complex. *ACS Appl. Mater. Interfaces* **2014**, *6*, 6005−6021.

(19) Li, C.; Benicewicz, B. C. Synthesis of Well-Defined Polymer Brushes Grafted onto Silica Nanoparticles via Surface Reversible Addition-Fragmentation Chain Transfer Polymerization. *Macromolecules* **2005**, *38*, 5929−5936.

(20) Edmondson, S.; Osborne, V. L.; Huck, W. T. S. Polymer Brushes via Surface-Initiated Polymerizations. *Chem. Soc. .Rev.* **2004**, *33*, 14−22.

(21) Chen, J.; Liu, M.; Chen, C.; Gong, H.; Gao, C. Synthesis and Characterization of Silica Nanoparticles with Well-Defined Thermoresponsive PNIPAM via a Combination of RAFT and Click Chemistry. *ACS Appl. Mater. Interfaces* **2011**, *3*, 3215−3223.

(22) Stöber, W.; Fink, A.; Bohn, E. Controlled Growth of Monodisperse Silica Spheres in the Micro Size Range. *J. Colloid Interface Sci.* **1968**, *26*, 62−69.

(23) Yang, J. J.; El-Nahhal, I.; Chuang, I.; Maciel, G. E. Synthesis and Solid-State NMR Structural Characterization of Polysiloxane-Immobilized Amine Ligands and their Metal Complexes. *J. Non-Cryst. Solids* **1997**, *209*, 19−39.

(24) Beganskienė, A.; Sirutkaitis, V.; Kurtinaitienė, M.; Juškėnas, R.; Kareiva, A. FTIR, TEM and NMR Investigations of Stöber Silica Nanoparticles. *Mater. Sci.* **2004**, *10*, 287−290.

(25) Sannigrahi, A.; Ghosh, S.; Lalnuntluanga, J.; Jana, T. How the Monomer Concentration of Polymerization Influences Various Properties of Polybenzimidazole: A Case Study with Poly(4,4′-Diphenylether-5,5′-bibenzimidazole). *J. Appl. Polym. Sci.* **2009**, *111*, 2194−2203.

(26) Singha, S.; Jana, T. Effect of Composition on the Properties of PEM Based on Polybenzimidazole and Poly(Vinylidene Fluoride) Blends. *Polymer* **2014**, *55*, 594−601.

(27) Akcora, P.; Liu, H.; Kumar, S. K.; Moll, J.; Li, Y.; Benicewicz, B. C.; Schadler, L. S.; Acehan, D.; Panagiotopoulos, A. Z.; Pryamitsyn, V.; Ganesan, V.; Ilavsky, J.; Thiyagarajan, P.; Colby, R. H.; Douglas, J. F. Anisotropic Self-Assembly of Spherical Polymer-Grafted Nanoparticles. *Nat. Mater.* **2009**, *8*, 354−359.

(28) Xiao, L.; Zhang, H.; Jana, T.; Scanlon, E.; Chen, R.; Choe, E. W.; Ramanathan, L. S.; Yu, S.; Benicewicz, B. C. Synthesis and Characterization of Pyridine Based Polybenzimidazole for High Temperature Polymer Electrolyte membrane Fuel Cells Applications. *Fuel Cells* **2005**, *5*, 287−295.
(29) Xiao, L.; Zhang, H.; Scanlon, E.; Ramanathan, L. S.; Choe, E. W.; Rogers, D.; Apple, T.; Benicewicz, B. C. High-Temperature Polybenzimidazole Fuel Cell Membranes via a Sol-Gel Process. *Chem. Mater.* **2005**, *17*, 5328−5333.
(30) Li, X.; Chen, x.; Benicewicz, B. C. Synthesis and Properties of Phenylindane-containing Polybenzimidazole (PBI) for High-Temperature Polymer Electrolyte Membrane Fuel Cells (PEMFCs). *J. Power Sources* **2013**, *243*, 796−804.
(31) Chuang, S.; Hsu, S. L.; Hsu, C. Synthesis and Properties of Fluorine-containing Polybenzimidazole/Montmorillonite Nanocomposite Membranes for Direct Methanol Fuel Cell Applications. *J. Power Sources* **2007**, *168*, 172−177.
(32) Suryani; Liu, Y. Preparation and Properties of Nanocomposite Membranes of Polybenzimidazole/ Sulfonated Silica Nanoparticles for Proton Exchange Membranes. *J. Membr. Sci.* **2009**, *332*, 121−128.
(33) Li, C.; Sun, G.; Ren, S.; Liu, J.; Wang, Q.; Wu, Z.; Sun, H.; Jin, W. Casting Nafion-Sulfonated Organosilica Nanocomposite Membranes Used in Direct Methanol Fuel Cells. *J. Membr. Sci.* **2006**, *272*, 50−57.
(34) He, R.; Li, Q.; Bach, A.; Jensen, J. O.; Bjerrum, N. J. Physicochemical Properties of Phosphoric Acid Doped Polybenzimidazole Membranes for Fuel Cells. *J. Membr. Sci.* **2006**, *277*, 38−45.
(35) He, R.; Li, Q.; Xiao, G.; Bjerrum, N. J. Proton Conductivity of Phosphoric Acid Doped Polybenzimidazole and its Composites with Inorganic Proton Conductors. *J. Membr. Sci.* **2003**, *226*, 169−184.